JOURNAL OF MATERIALS SCIENCE 32 (1997) 6311–6315

Hydrogen diffusivity and solubility in crystalline and amorphous alloys

D. S. DOS SANTOS, P. E. V. DE MIRANDA
COPPE-EE, Universidade Federal do Rio de Janeiro, CP 68505, CEP 21945-970, Rio de Janeiro, RJ Brazil

The hydrogen permeation behaviour of iron- and nickel-based amorphous alloys was characterized using electrochemical methodology and compared with the properties of crystalline metals and alloys. The materials studied were amorphous $Fe_{40}Ni_{38}Mo_4B_{18}$, $Fe_{74}Ni_4Mo_3B_{17}$, $Fe_{78}B_{13}Si_9$ and $Ni_{81}P_{19}$, as well as a crystalline low-carbon steel, pure nickel and pure palladium. The double potentiostatic electrochemical hydrogen permeation tests were performed at 40 °C using a 0.1 N NaOH solution as electrolyte. It was found that the hydrogen diffusivity in the iron-based amorphous alloys is a few orders of magnitude lower than in carbon steel and iron, while a much smaller difference exists between $Ni_{81}P_{19}$ and pure nickel. Furthermore, the amorphous alloys showed a strikingly greater capacity to dissolve hydrogen in solid solution compared with their crystalline counterparts. In some cases, their apparent hydrogen solubility was even greater than that for the liquid metal of the main element present in their chemical composition.

1. Introduction

The interaction of hydrogen with the structure of metals and alloys has been a subject of considerable scientific interest for many years. Such interest arose because this element, when present in solid solution, even at small concentrations, in metallic materials, can result in significant changes in the mechanical and metallurgical properties, provoking hydrogen embrittlement. This deleterious characteristic of hydrogen with respect to metallic materials is facilitated by its tendency to segregate to those regions in the microstructure which exhibit potential energies higher than that of the normal sites in the atomic lattice, thereby becoming preferential positions for hydrogen segregation and trapping. Examples of such hydrogen segregation sites include dislocations and associated substructures, microvoids, internal free surfaces (pores) and precipitate–matrix interfaces, among other common defects of the metallic structure [1].

The study of the behaviour of hydrogen in amorphous metallic materials was prompted by the observation of the alterations that this element can cause in the physicochemical, mechanical and metallurgical properties of these materials. Furthermore there exists a promising potential, because of their elevated capacity to retain hydrogen in solid solution [2]. This has, in recent years, attracted the attention of a large number of researchers in various fields, who have worked towards the common objective of discovering safe alternative means for the storage of high-energy-content products, without adverse repercussions for the environment. Another important aspect of the study of hydrogen in amorphous materials is that related to the utilization of hydrogen as a probe in the analysis and investigation of structural disorder in this class of new materials [3].

In the conventional crystalline materials, hydrogen dissolves principally in the tetrahedral interstitial sites in body-centred cubic structures and in the octahedral interstitial sites in face-centred cubic (f.c.c.) structures. The presence of defects in metallic microstructures, which act as hydrogen traps, results in a significant reduction in hydrogen mobility since hydrogen tends to diffuse to these defects and becomes bonded to them. These same defects, however, contribute to the increased number of hydrogen dissolution sites, which effectively increases the apparent hydrogen solid solubility.

The elevated cooling rates utilized during the fabrication of amorphous metals generate innumerable defects of different potential energies in the metallic structure. Such defects, generated by rapid solidification, are not comparable with those present in the crystalline structure of the conventional metals, the amorphous structure being more similar to the structure of molten metals. The high defect content contributes to a large increase in the solid solubility of hydrogen and a reduction in its diffusivity.

In general, for the crystalline metals and metallic alloys, the hydrogen diffusivity does not vary with increasing concentration of hydrogen in solid solution, while in the amorphous metals a strong concentration dependence is evident for hydrogen diffusivity. This is largely due to the structural disorder of these metals. Kirchheim [3] observed experimentally that the distribution of the hydrogen atoms among the different energy sites in the amorphous structure can be modelled using Fermi–Dirac statistics and that the

0022–2461

relationship between diffusivity and hydrogen concentration follows a distribution which approximates well to a Gaussian function.

The current work has as its objective the characterization of the hydrogen permeation behaviour in iron- and nickel-based amorphous metallic ribbons produced by melt spinning, by determining the hydrogen flux, apparent diffusivity and apparent solubility, with the aim of comparing these data with those obtained for crystalline metals and alloys.

2. Experimental techniques

The four amorphous metallic ribbons 25.4 mm wide utilized in this work, $Fe_{40}Ni_{38}Mo_4B_{18}$, $Fe_{74}Ni_4Mo_3B_{17}$, $Fe_{78}B_{13}Si_9$ and $Ni_{81}P_{19}$, were produced by melt spinning with thicknesses of 25 μm, 25 μm, 20 μm and 55 μm, respectively. By means of comparison, additional samples of crystalline materials were prepared of pure nickel (heat treated for 3 h at 380 °C), pure palladium (heat treated for 1 h at 820 °C) and as-received low-carbon steel sheet. Samples of each material, in the as-received condition (amorphous alloys and carbon steel) or heat treated (nickel and palladium), were submitted to electrochemical hydrogen permeation tests, as described elsewhere [4]. The applied hydrogen generation potentials were − 1.1 V with respect to a saturated calomel electrode (SCE) for palladium, − 1.35 V (SCE) for the iron-based alloys and − 1.65 V (SCE) for the $Ni_{81}P_{19}$ alloy and pure nickel. These tests were undertaken using an electrochemical cell comprising two compartments separated by the sample under examination (Fig. 1). The tests were conducted at 40 °C, using a 0.1 N NaOH electrolyte in both compartments of the cell. Nitrogen bubbling was maintained in both compartments to minimize the level of dissolved oxygen in the solution, thereby guaranteeing more precise measurements of the anodic current. In one of the compartments, the hydrogen generation side, a constant cathodic potential was applied to generate hydrogen on the surface of the metal. Most of the hydrogen thus generated is absorbed by the metal surface and subsequently diffuses across the sample thickness. In the other compartment, a slightly anodic potential was applied so as to maintain a zero hydrogen concentration on that surface. The arrival of hydrogen in the detection compartment of the electrochemical cell produces a current which increases with increasing hydrogen flux as a function of time until steady-state conditions are achieved. Each of the electrons (e^-) responsible for the generation of the anodic current corresponds to one of the hydrogen atoms leaving the metal, according to the chemical reaction

$$\tfrac{1}{2}H_2 \rightarrow H^+ + e^- \quad (1)$$

The evolution of the anodic current, $i(t)$, with time, t, exhibits a sigmoidal relationship. On the assumption that the diffusivity of hydrogen does not vary with the increase in concentration, the current may be expressed as [5]

$$i_L(t) = i_\infty \left[1 + 2 \sum_1^n (-1)^n \exp\left(\frac{-n^2\pi^2 D_{app} t}{L^2} \right) \right] \quad (2)$$

where i_∞ is the steady-state current, D_{app} is the apparent hydrogen diffusivity, L is the sample thickness and $n = 1, 2, 3, \ldots$. D_{app} is determined by the best fit of the experimental data to Equation 2. The hydrogen flux $J_L(t)$ which permeates the metal is proportional to the permeation current as defined by Faraday's law:

$$J_L(t) = \frac{i_L(t)}{zFA} \quad (3)$$

where z is the number of electrons participating in the reaction, F is the Faraday constant and A is the sample area exposed to the electrolyte. The hydrogen-flux-to-diffusivity ratio multiplied by the sample thickness provides the apparent hydrogen solubility, S_{app},

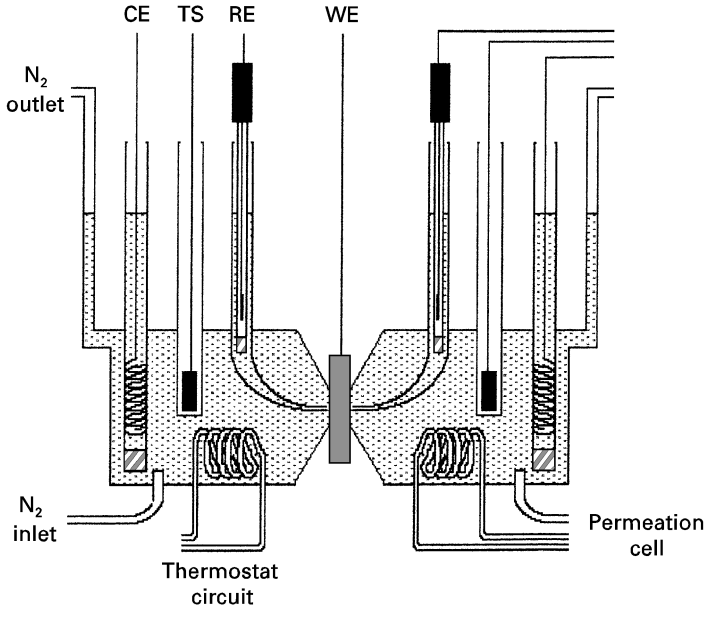

Figure 1 Schematic representation of the cell used in the hydrogen permeation tests. CE, counter-electrode; TS, temperature sensor; RE, reference electrode; WE, work electrode.

of the material at steady state as follows:

$$S_{app} = \frac{J_\infty L}{D_{app}} \quad (4)$$

3. Results

The hydrogen permeation curves for the amorphous alloys tested at 40 °C are presented in Fig. 2 for the $Ni_{81}P_{19}$ alloy and in Fig. 3 for the iron-based alloys ($Fe_{40}Ni_{38}Mo_4B_{18}$, $Fe_{74}Ni_4Mo_3B_{17}$ and $Fe_{78}B_{13}Si_9$). For each alloy these figures show the experimental data points and a solid curve, which represents the best fit of the experimental data to Equation 2. This fitting was used to determine the apparent hydrogen diffusion coefficient in each case. It is clear that the hydrogen flux at steady state for the nickel-based amorphous alloy is about an order of magnitude greater than that for the iron-based amorphous alloys. Also the iron-based alloy containing more nickel presents an increased hydrogen flux. Table I depicts the hydrogen permeation parameters obtained for the amorphous and crystalline materials studied. Discrete values for the hydrogen diffusivity, flux and solubility are presented for each material at 40 °C, as well as the sample thicknesses.

4. Discussion

The hydrogen diffusion coefficient in solid metallic amorphous alloys is dependent on concentration, because of the presence of structural sites possessing different levels of potential energy for hydrogen localization and diffusion [3]. At low hydrogen concentrations the hydrogen atoms preferentially fill the higher- energy sites, leading to a marked decrease in their mobility. As the high-potential-energy defects approach maximum coverage with increasing concentration, their influence on the hydrogen mobility decreases, permitting the hydrogen diffusion coefficient to increase. Sakamoto *et al.* [6] have found for $Ni_{80}P_{20}$ that the hydrogen diffusion coefficient increases abruptly with increasing hydrogen concentration, eventually approaching a plateau for higher concentration values. These workers have performed galvanostatic–potentiostatic hydrogen permeation tests, instead of the potentiostatic–potentiostatic-type tests used in the present work. In their case the use of very small hydrogen generation currents in some tests has permitted to derive the smaller hydrogen diffusion coefficients, by allowing small amounts of hydrogen to be absorbed by specimen. They observed that small increases in the hydrogen generation current (i.e., hydrogen concentration) rapidly lead to higher values of the hydrogen diffusion coefficient. On the other hand, the high cathodic potential level used in the double potentiostatic experiments performed in the present work represented an elevated current for the cathodic generation of hydrogen (equal to 70 A m^{-2}). Therefore, all tests herein described were conducted in such a condition that the potential energy sites for hydrogen localization in the amorphous structure were saturated by hydrogen as the hydrogen permeation test proceeded. Since this involves higher hydrogen concentrations and higher coverages, the energy potential sites become progressively prevented from influencing the hydrogen diffusivity. Therefore, the hydrogen diffusion coefficients shown herein present a very small variation with concentration, for which Fick's law of diffusion is a good approximation. The hydrogen diffusion coefficients depicted in Table I were determined by the best fit of the experimental results to Equation 2, which is a solution of Fick's second law for the present case. It may be observed that the iron-based amorphous alloys have a very small hydrogen diffusion coefficient compared with that of low-carbon steel. Being an f.c.c. material, nickel has a very low D_{app}, not differing very much from that of the amorphous $Ni_{81}P_{19}$ alloy. The kinetics of hydrogen permeation in these materials is, however, better described by the graphs in Fig. 4. This

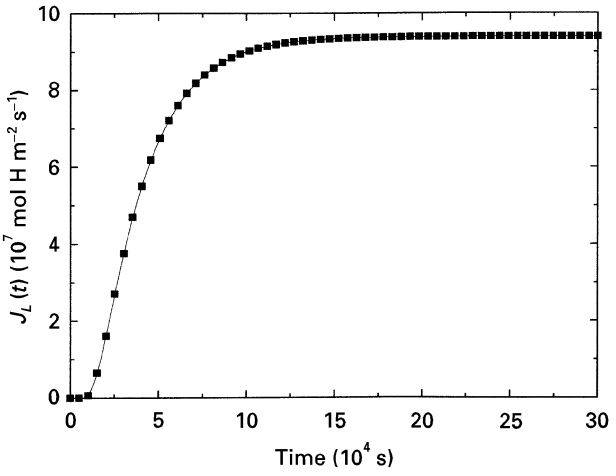

Figure 2 Hydrogen permeation curve for amorphous $Ni_{81}P_{19}$ at 40 °C.

TABLE I Hydrogen permeation parameters at 40 °C

Material	D_{app} (m^2 s^{-1})	J_∞ (mol H m^2 s^{-1})	S_{app} (mol H m^{-3})	L (m)
$Fe_{40}Ni_{38}Mo_4B_{18}$	2.0×10^{-14}	1.4×10^{-7}	170.0	2.5×10^{-5}
$Fe_{78}B_{13}Si_9$	4.1×10^{-15}	7.8×10^{-8}	380.0	2.0×10^{-5}
$Fe_{74}Ni_4Mo_3B_{17}Si_2$	2.7×10^{-15}	1.2×10^{-8}	88.0	2.5×10^{-5}
$Ni_{81}P_{19}$	1.2×10^{-14}	9.4×10^{-7}	4250.0	5.5×10^{-6}
Ni	4.4×10^{-14}	1.0×10^{-7}	113.0	4.8×10^{-5}
Pd	6.3×10^{-11}	4.3×10^{-5}	300.0	4.2×10^{-4}
Low-C steel	6.7×10^{-10}	8.0×10^{-7}	1.1	1.0×10^{-3}

presents curves of hydrogen flux, normalized for the steady state flux (at the plateaux shown in Figs 2 and 3), as a function of a non-dimensional parameter, τ, which takes into account the hydrogen diffusion coefficient and the thickness of the specimen. Going from pure iron to the iron-based amorphous alloys, passing by the commercial carbon steel, one may observe that the kinetics of hydrogen permeation becomes slower the greater the amount of defects in the structure considered. That is, as mentioned before, the presence of defects in the structure, possessing different levels of potential energy to trap hydrogen as it wanders about its diffusion path, effectively influences its mobility, decreasing D_{app} with the increase in the amount of defects. Slower kinetics of diffusion are observed for the very defective amorphous $Ni_{81}P_{19}$ alloy, made from a main constituent (nickel) in which the hydrogen diffusivity in the crystalline state is already very small (Table I).

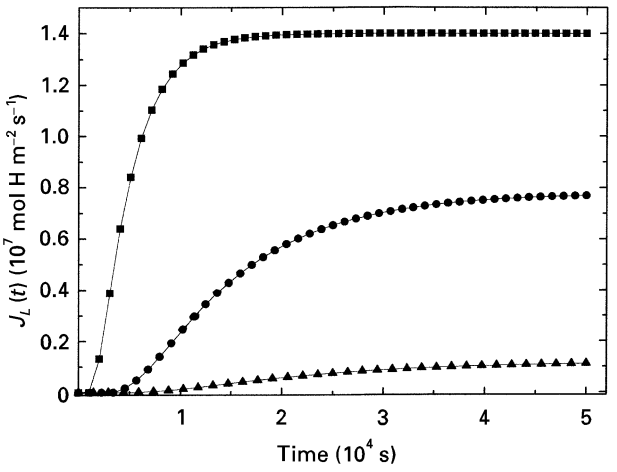

Figure 3 Hydrogen permeation curves for amorphous iron-based alloys at 40 °C. (■), $Fe_{40}Ni_{38}Mo_4B_{18}$; (●), $Fe_{78}B_{13}Si_9$; (▲), $Fe_{74}Ni_4Mo_3B_{17}Si_2$

On the basis of previously obtained potentiodynamic polarization curves for each material, under the same conditions (electrolyte and temperature) that the hydrogen permeation tests were planned to be performed, the cathodic hydrogen generation potential used in the latter were chosen so as to have the same cathodic current in all tests. This assured equal fugacities, i.e., similar amounts of hydrogen available to be absorbed by and to diffuse throughout the samples. Although the apparent hydrogen diffusion coefficients herein determined are not expected to depend on the different cathodic potentials used for hydrogen generation in the hydrogen permeation tests for each material, this is not the case for the measurements of apparent hydrogen solubilities. It has been shown [7] that the hydrogen flux at steady state (i.e., in the plateau of the curves shown in Figs 2 and 3) for amorphous alloys is highly dependent on the experimental conditions used in the hydrogen permeation test, increasing with increase in the cathodic potential (or current) used for hydrogen generation. Hence, the S_{app} values presented in this work are characteristic of the experimental conditions at

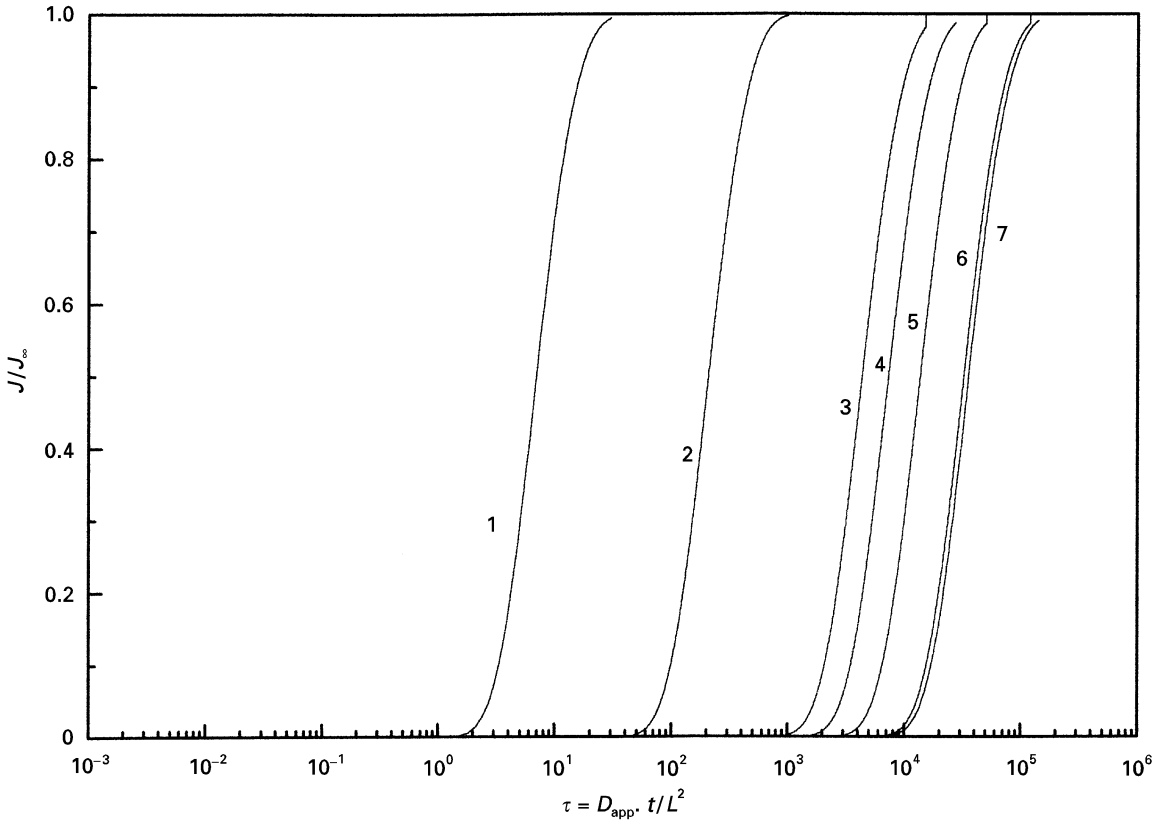

Figure 4 Hydrogen flux normalized by its value at steady state as a function of τ for different crystalline and amorphous materials. Curve 1, pure crystalline iron; curve 2, low-carbon steel; curve 3, $Fe_{40}N_{38}Mo_4B_{18}$; curve 4, $Fe_{78}B_{13}Si_9$, curve 5, nickel; curve 6; $Fe_{74}Ni_4Mo_3B_{17}Si_2$; curve 7, $Ni_{81}P_{19}$.

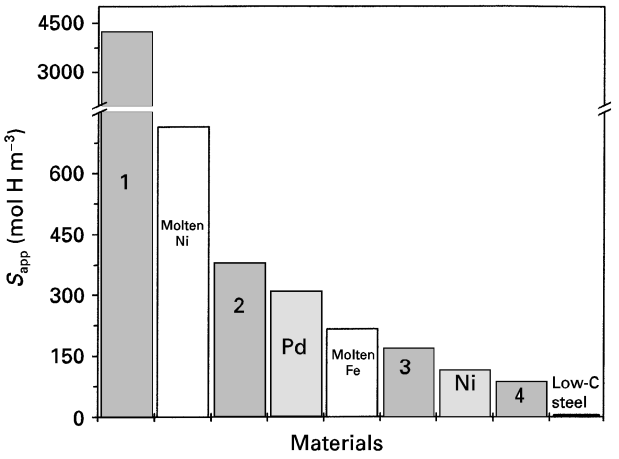

Figure 5 Hydrogen solubility for different crystalline (□) and amorphous (■) metallic alloys at 40 °C and for molten nickel and iron (□). 1, $Ni_{81}P_{19}$; 2, $Fe_{78}B_{13}Si_9$; 3, $Fe_{40}Ni_{38}Mo_4B_{18}$; 4, $Fe_{74}Ni_4Mo_3B_{17}Si_2$.

present used. Also, it is important to remark that the hydrogen solubility is here considered to be the total amount of hydrogen kept in the sample's structure either in interstitial solid solution or bound to defects.

Taking this into consideration, the apparent solubility of hydrogen in different materials may be compared by analysis of Fig. 5. It shows that the apparent hydrogen solubility in the $Ni_{81}P_{19}$ solid amorphous alloy at 40 °C is approximately six times greater than that found for molten nickel [8] and about 40 times more than in solid annealed crystalline nickel at 40 °C. Also one of the iron-based solid amorphous alloys ($Fe_{78}B_{13}Si_9$) presents a higher apparent hydrogen solubility at 40 °C than molten iron [8]. This similarity between the behaviours (high hydrogen solubility) of amorphous alloys and their corresponding pure metals in the molten state is further supported by other techniques, particularly that presented by Vatolin *et al.* [9]. These workers showed, by an analysis of X-ray diffraction peaks in the radial distribution function, a correspondence between the potential energy distribution functions for iron in the liquid and the amorphous states and the contrast between these and those for the solid state. This analysis confirmed their supposition that the solid amorphous alloys exhibit properties of the materials in the liquid state. The apparent hydrogen solubility in $Fe_{78}B_{13}Si_9$ reaches about 40 000 times that of pure crystalline iron [10], being even greater than that in palladium, a metal known for its special properties with hydrogen.

5. Conclusions

Electrochemical hydrogen permeation tests performed at 40 °C, using amorphous and crystalline metals and alloys indicate that the hydrogen diffusivity is lower in amorphous materials than in their crystalline counterparts. The hydrogen diffusion coefficient of the iron-based alloys $Fe_{40}Ni_{38}Mo_4B_{18}$, $Fe_{74}Ni_4Mo_3B_{17}$ and $Fe_{78}B_{13}Si_9$ is several orders of magnitude lower than that of low-carbon steel and pure iron, while a much smaller difference exists between the values for the hydrogen diffusivity in $Ni_{81}P_{19}$ and pure nickel. It is also observed that the amorphous alloys dissolve greater amounts of hydrogen in solid solution and, in some cases, even more than the liquid metal of the element present in the major quantity in their chemical composition.

Acknowledgements

The authors acknowledge the Allied Signal Co., for the kind donation of the experimental amorphous alloys herein used and the Conselho Nacional de Desenvolvimento Científico e Tecnológico (grants 523697/94-5 and PADCT 620114/92-4) for financial support of this research.

References

1. J. P. HIRTH, *Metall. Trans. A* **11** (1980) 861.
2. D. MENZEL, A. NIKLAS and U. KOSTER, *Mater. Sci. Engng* **A133** (1991) 312.
3. R. KIRCHHEIM, *Prog. Mater. Sci.* **32** (1988) 262.
4. A. H. BOTT, D. S. DOS SANTOS and P. E. V. DE MIRANDA, *J. Mater. Sci. Lett.* **12** (1993) 390.
5. N. BOES and H. ZÜCHNER, *J. Less-Common Metals* **49** (1976) 223.
6. Y. SAKAMOTO, K. TAKAO and K. BABA, *Mater. Sci. Engng* **97** (1988) 437.
7. D. S. DOS SANTOS and P. E. V. DE MIRANDA, *Matéria* **2** (1) (1997) http: //www.coppe.ufrj.br/~notimat/materia/Vol 2N1/artigo.htm (Virtual Journal).
8. W. M. MUELLER, J. P. BLACKLEDGE and G. G. LIBOWITZ (eds) "Metal hydrides" (Academic Press, New York, 1968).
9. N. A. VATOLIN, V. A. POLUKHIN, R. M. BELYAKOVA and E. A. PASTUKHOV, *Mater. Sci. Engng* **99** (1988) 551.
10. A. J. KUMMNICK and H. H. JOHNSON, *Acta Metall.* **33** (1980) 28.

Received 8 December 1995
and accepted 10 March 1997